Research Square

Preprints are preliminary reports that have not undergone peer review.
They should not be considered conclusive, used to inform clinical practice,
or referenced by the media as validated information.

Habitat Analysis of the Peritumoral Edema Region Combined with Visually Accessible Rembrandt Images Features and the Intratumoral Heterogeneity Score for Preoperative Prediction of Isocitrate Dehydrogenase Status in Adult-Type Diffuse Glioma: A Two-Center Study

Sijia Li[1]
The First Affiliated Hospital of Xinjiang Medical University
Wei Zhao[2]
The Fourth Affiliated Hospital of Xinjiang Medical University
Rui Xu[1]
The First Affiliated Hospital of Xinjiang Medical University
Kukun Hangaerbieke[1]
The First Affiliated Hospital of Xinjiang Medical University
Jingming Jiang[1]
The First Affiliated Hospital of Xinjiang Medical University
Subi Yimuran[1]
The First Affiliated Hospital of Xinjiang Medical University
Yunling Wang
doctorwang1005@163.com

The First Affiliated Hospital of Xinjiang Medical University

Research Article

Keywords: Adult-Type Glioma, Isocitrate Dehydrogenase, Habitat Analysis, VASARI Features, Machine Learning

Posted Date: November 20th, 2026

DOI: https://doi.org/10.21203/rs.3.rs-11111225/v1

License: This work is licensed under a Creative Commons Attribution 4.0 International License.
Read Full License

Additional Declarations: No competing interests reported.

Abstract

Purpose: To develop and validate magnetic resonance imaging (MRI)-based machine learning models integrating habitat analysis of peritumoral edema regions, Visually Accessible Rembrandt Images (VASARI) features and intratumoral heterogeneity (ITH) score for preoperative prediction of isocitrate dehydrogenase (IDH) status in adult-type diffuse glioma.

Methods: This retrospective study included 606 patients with adult-type diffuse glioma from two centers (376 for development; 230 for external validation). The peritumoral edema region was divided into two habitats (H1 and H2) using *K*-means clustering. Habitat-derived radiomics features, VASARI features, and the ITH score were used to construct five models: H1, H2, H1+H2, VASARI + ITH, and a comprehensive fusion model. Model performance was evaluated using the area under the receiver operating characteristic curve (AUC), accuracy, sensitivity, and specificity. Shapley Additive Explanations (SHAP) method was employed for interpretability analysis.

Results

The H2 model outperformed H1 model (AUC, 0.884 vs 0.773). The VASARI + ITH model achieved an AUC of 0.841, whereas the H1 + H2 model achieved an AUC of 0.890. The comprehensive fusion model exhibited the best AUC (0.892), accuracy, sensitivity, and specificity. SHAP analysis revealed that habitat-derived radiomic features contributed most to model prediction.

Conclusion

A fusion model combining habitat-derived radiomics features from the glioma peritumoral edema region, VASARI features, and the ITH score demonstrated favorable predictive performance for preoperative prediction of IDH status in adult-type diffuse glioma.

Introduction

Glioma accounts for approximately 40%-60% of all primary central nervous system (CNS) tumors [1]. The latest edition of the World Health Organization (WHO) classification of CNS tumors integrated molecular criteria into tumor definitions, and the mutational status of isocitrate dehydrogenase (IDH) is now the principal discriminator among adult-type diffuse gliomas, which are classified as astrocytoma, IDH-mutant; oligodendroglioma, IDH-mutant and 1p/19q codeletion; or glioblastoma, IDH-wildtype [2]. IDH status determines prognosis, influences the extent of resection that is pursued and defines eligibility for IDH-inhibitor therapy. At present it can be established only from tissue samples obtained via invasive biopsy or surgical resection [3, 4], limiting the feasibility of early preoperative assessment. A reliable noninvasive method for predicting before surgery holds significant clinical importance [5].

Magnetic resonance imaging (MRI) is the reference imaging modality for the preoperative assessment of gliomas, and radiomics analysis of MRI has been widely investigated as a surrogate of molecular

features [6]. However, traditional radiomics analysis typically extracts average features based on the entire tumor region, which may not adequately reflect the complex spatial heterogeneity. Glioma subregions differ substantially in vascular permeability, cell density, and tumor microenvironment [7], thereby shaping the imaging expression of molecular phenotypes. Analytical strategies that preserve, rather than average out, this spatial information may therefore improve the noninvasive prediction of IDH status.

Habitat analysis addresses this limitation by applying clustering to voxelwise signal pattern, thereby partitioning a tumor lesion into subregions (habitats) that are presumed to correspond to distinct pathophysiological characteristics [8], and has been applied to molecular subtyping, outcome prediction [9, 10], and IDH status prediction in gliomas [11–13]. Most published habitat models, however, rely on advanced MRI sequences and post-processing, such as perfusion, diffusion kurtosis or metabolic imaging, which are not universally available and prolong examination times. Moreover, these studies have focused mainly on the contrast-enhancing tumor, whereas the peritumoral edema region receives relatively little attention. This region contains both vasogenic edema and infiltrating tumor cells and thus may reflect microenvironmental variations associated with IDH status. Habitat analysis of the peritumoral region using conventional MRI may therefore capture IDH-related heterogeneity that whole-lesion analysis may overlook.

In addition, two complementary descriptors may further enrich such a model. Visually Accessible Rembrandt Images (VASARI) features provide a standardized description of glioma morphology, margins, enhancement, necrosis, and edema, reflecting macroscopic phenotype [14]. The intratumoral heterogeneity (ITH) score quantifies spatial fragmentation of imaging habitats and provides a single continuous measure of intratumoral heterogeneity. We hypothesized that integrating habitat radiomics of the peritumoral edema region with VASARI features and the ITH score would improve the preoperative prediction of IDH status. Accordingly, we developed such models using only conventional MRI sequences and evaluated them in an independent external validation cohort.

Materials and Methods

Study Design and Patients

This retrospective study was approved by the Medical Ethics Committee of the First Affiliated Hospital of Xinjiang Medical University (approval number K202405-48), and the requirement for written informed consent was waived because of the retrospective design. The study was conducted in accordance with the ethical standards laid down in the 1964 Declaration of Helsinki and its later amendments. We reviewed consecutive adult patients with pathologically confirmed glioma who underwent stereotactic biopsy or surgical resection at center A $n = 376$ and center B $n = 230$ between January 2019 and March 2024.

Inclusion criteria: i) grade II-IV gliomas according to the WHO 2021 classification of central nervous system tumors; ii) complete preoperative MRI data comprising T1-weighted imaging (T1WI), T2-weighted imaging (T2WI), T2-weighted fluid-attenuated inversion recovery (T2-FLAIR) and contrast-enhanced T1-weighted imaging (CE-T1WI) of diagnostic quality; iii) no prior antitumor treatment before index MRI examination.

Exclusion criteria: i) history of neurosurgical procedures; ii) patients with concomitant heart, liver, or kidney dysfunction.

The 376 patients from center A formed development cohort and were randomly assigned to a training set and an internal validation set in a 7:3 ratio (97 IDH-mutant and 279 IDH-wildtype), and the 230 patients from center B served as an external validation set (68 IDH-mutant and 162 IDH-wildtype). IDH status was determined by immunohistochemistry (IHC) analysis of postoperative pathological specimens.

Image Acquisition

MRI examinations were conducted on two 3.0T scanners: Signa Architect, GE Healthcare (*n* = 376); Ingenia CX, Philips Healthcare (*n* = 230). The protocol comprised T1-weighted imaging (T1WI), T2-weighted imaging (T2WI), T2-weighted fluid-attenuated inversion recovery (T2-FLAIR), and contrast-enhanced T1-weighted imaging (CE-T1WI). Detailed acquisition parameters for each sequence are presented in Table 1. A gadolinium-based contrast agent was administered intravenously at a dose of 0.15 mmol/kg and a flow rate of 3.0 mL/s, and CE-T1WI was acquired with the same parameters as unenhanced T1WI.

Table 1
MRI Acquisition Parameters for the Two Scanners

Sequence	Parameters	GE Signa Architect	Philips Ingenia CX
T1WI	Pulse sequence	FSE	GRE
	Echo time(TE)	24ms	2ms
	Repetition time(TR)	200ms	600ms
	Matrix	256×256	256×256
	Slice thickness	6mm	5mm
T2WI	Pulse sequence	FSE	SE
	Echo time(TE)	102ms	100ms
	Repetition time(TR)	3808ms	2800ms
	Matrix	256×256	256×256
	Slice thickness	6mm	5mm
T2-FLAIR	Pulse sequence	IR	IR
	Echo time(TE)	126ms	256ms
	Repetition time(TR)	7000ms	4800ms
	Matrix	256×256	256×256
	Slice thickness	6mm	5mm

Note. FSE = fast spin echo, GRE = gradient recalled echo, IR = inversion recovery, SE = spin echo, TE = echo time, TR = repetition time.

Image Processing and Segmentation

All images underwent identical preprocessing. N4 bias field correction was performed using ITK-SNAP software (http://www.itksnap.org), and T1WI and CE-T1WI were registered to T2WI. Images were normalized by z-score normalization using PyRadiomics (http://pyradiomics.readthedocs.io) and resampled to an isotropic voxel size of 1 × 1 × 1 mm^3 with linear interpolation in SimpleITK.

For segmentation, a three-dimensional full-resolution nnU-Net model was used to automatically segment the peritumoral edema region on T2WI images, generating an initial mask. Two radiologists with 8 and 12 years of experience in neuro-oncologic diagnosis independently corrected the automated segmentation mask, editing missed, over-segmented,and boundary-deviated regions slice by slice.After the correction, the two radiologists discussed the discrepant regions until consensus was reached ,and the final gold-standard segmentation mask was generated.

The region of interest (ROI) was defined as the peritumoral edema region, the region surrounding the tumor that is hyperintense on T2WI/T2-FLAIR and shows no enhancement on CE-T1WI. Delineation was performed using FLAIR as the primary reference sequence, in combination with T1WI and CE-T1WI, to exclude enhancing tumor parenchyma as well as necrotic and cystic areas. The outer boundary of the edema region was defined as the signal transition zone between the abnormal hyperintensity and the normal brain parenchyma.

Determination of the Number of Habitats

Voxels within the peritumoral edema region were clustered with the *K*-means algorithm. The optimal number of habitats was determined with the Calinski-Harabasz index, which reached its maximum at $K = 2$. Accordingly, the edema region was partitioned into two habitats, designated H1 and H2.

Feature Extraction

Radiomic features were extracted with PyRadiomics from each habitat of the four sequences, yielding 7868 features per patient: 1512 first-order features, 56 shape features, and 6,300 texture features.

VASARI features were assessed independently on CE-T1WI by two neuroradiologists with 8 and 12 years of experience who were blinded to the histopathologic and molecular findings; disagreements were resolved by consensus.

The ITH score was derived from the habitat maps based on the spatial distribution of connected components within each habitat [15]. Higher ITH scores indicated greater habitat fragmentation and thus greater intratumoral heterogeneity.

Feature Selection

Missing values were imputed with the training-set median. Features with a variance below 1×10^{-8} were discarded as non-informative. Highly correlated redundant features with Pearson correlation coefficient greater than 0.995 were eliminated, and the remaining features were standardized to a uniform scale using Z-score normalization. The Boruta algorithm was employed to retain features that were consistently associated with IDH status. These features were ranked by the minimum redundancy maximum relevance criterion, and the top 40 features were carried forward. Feature stability and relative importance were finally assessed using random forest models with bootstrap resampling.

Model Development and Validation

Five models were developed: i) an H1 habitat model, ii) an H2 habitat model, iii) an H1 + H2 fusion model, iv) a VASARI + ITH score model, and v) a comprehensive model combining habitat radiomics, VASARI

features and the ITH score. To select the optimal classifier, four algorithms (CatBoost, elastic net, LightGBM, and XGBoost) were compared using the H1 + H2 feature set within the training set by five-times-repeated 10-fold cross-validation. The best-performing classifier was then adopted for all subsequent models. Model performance was summarized with the area under the receiver operating characteristic curve (AUC), accuracy, F1 score, sensitivity and specificity. The complete workflow is shown in Fig. 1.

Statistical Analysis

Clinical and demographic comparisons were performed using SPSS 27.0. Continuous variables were presented as mean ± standard deviation and were compared with the independent samples t test when normally distributed and with the Mann-Whitney U test otherwise; normality was assessed with the Shapiro-Wilk test. Categorical variables were expressed as counts (percentages) and were compared with the Chi-square test or Fisher's exact test. Receiver operating characteristic and precision-recall analyses, calibration curves and all performance metrics were computed in Python 3.12. Ninety-five percent confidence intervals for the AUC were obtained by bootstrapping with 1000 resamples, and AUCs of competing models were compared with the DeLong test. Two-tailed *P* values less than .05 were considered to indicate statistical significance.

Results

Patient Characteristics

IDH-mutant tumors accounted for 97 of 376 (25.8%) tumors in the development cohort and 68 of 230 (29.6%) tumors in the external validation cohort. Age, sex, WHO grade, and IDH status did not differ significantly between the two cohorts (*P* = .25–.62; Table 2).

Table 2
Characteristics of the Development and External Validation Cohorts

Age	**Development cohort(*n* = 376)**	**External validation cohort(*n* = 230)**	***P*-value**
	50.89 ± 13.732	**51.45 ± 11.994**	**0.607**
Sex			0.248
Male	211(56.1%)	118(51.3%)	
Female	165(43.9%)	112(48.7%)	
WHO Grade			0.620
3	77(20.5%)	51(22.2%)	
4	299(79.5%)	179(77.8%)	
IDH			0.312
IDH-wildtype	279(74.2%)	162(70.4%)	
IDH-mutant	97(25.8%)	68(29.6%)	

Model Performance

Representative habitat maps of the peritumoral edema region and the 40 retained radiomic features ranked by random forest importance are shown in Fig. 2. Among the four classifiers evaluated, elastic net achieved the highest discrimination (AUC, 0.890; accuracy, 0.843) and was adopted for all subsequent models (Supplementary Table S1).

The H1, H2, H1 + H2, VASARI + ITH, and comprehensive fusion models achieved AUCs of 0.773, 0.884, 0.890, 0.841, and 0.892, respectively. The comprehensive fusion model yielded an accuracy of 0.843, a sensitivity of 0.750, and a specificity of 0.883. Calibration curves for the comprehensive fusion and H1 + H2 models lay close to the diagonal. On precision-recall analysis, the comprehensive fusion model achieved the highest average precision (0.772) (Fig. 3A–3C, Table 3).

Table 3
Performance of the Five Prediction Models

H1 model	**AUC**	**ACC**	**F1**	**Sensitivity**	**Specificity**
	0.773	**0.834**	**0.600**	**0.838**	**0.599**
H2 model	0.884	0.852	0.742	0.721	0.907
H1 + H2 fusion model	0.890	0.843	0.739	0.750	0.883
VASARI+ITHscore	0.841	0.822	0.732	0.824	0.821
Comprehensive fusion model	0.892	0.843	0.739	0.750	0.883

Model Interpretability

In the H1 habitat, CE-T1WI–derived texture features dominated the top contributors, followed by T2WI-derived features (Fig. 3D). In the H2 habitat, the most influential features were derived from CE-T1WI and T2-FLAIR, with dependence entropy recurring across multiple filter scales and sequences (Fig. 3E). Among the VASARI features, tumor location, definition of the enhancing margin, and enhancement quality contributed most to prediction (Fig. 3F). In the comprehensive fusion model, the SHAP values of the H1 + H2 radiomics score were widely distributed, whereas those of the VASARI score clustered narrowly around zero (Fig. 3G).

Discussion

In this two-center study, unsupervised habitat analysis of the peritumoral edema region on conventional MRI provided substantial information for preoperative IDH prediction. The H2 model outperformed the H1 model (AUC, 0.884 vs 0.773), combining the two habitats further improved discrimination (AUC, 0.890), and the comprehensive fusion model achieved the best overall performance (AUC, 0.892). These findings suggest that spatial heterogeneity within the peritumoral edema region contains informative imaging features related to IDH status.

The peritumoral edema region is not pure vasogenic edema but contains tumor cells infiltrating along white matter tracts [16–17]. Its biologic heterogeneity, reflected in differences in tumor cell density, microvascular architecture, and blood–brain barrier integrity [18], has been associated with tumor recurrence [19]. Radiomics of the peritumoral edema region, combined with habitat clustering, can capture and quantify this heterogeneity, thereby enabling imaging-based prediction of IDH status.

The divergent performance of the two habitats is biologically plausible. IDH mutation drives metabolic reprogramming and epigenetic dysregulation through the accumulation of 2-hydroxyglutarate, which inhibits α-ketoglutarate-dependent dioxygenases and produces global DNA and histone hypermethylation [20–21]; these alterations are linked to tumor cell differentiation state and proliferation rate [22]. IDH-mutant gliomas typically infiltrate diffusely but at lower cell density, grow more slowly, and undergo necrosis less frequently than IDH-wildtype tumors [23]. Such differences would be expected to manifest as reduced textural complexity in the peritumoral region of IDH-mutant tumors because distinct portions of the T2-FLAIR-hyperintense region correspond to different degrees of tumor cell infiltration [24], the superior performance of H2 may reflect greater sensitivity to regions of denser infiltration and microenvironmental alteration, whereas H1 may correspond more closely to vasogenic edema–dominant territory, in which signal changes reflect blood-brain barrier disruption and altered vascular permeability rather than tumor genotype [25].

The VASARI + ITH model alone achieved an AUC of 0.841, indicating that morphologic descriptors and the ITH score carry some IDH-related information. The comprehensive fusion model improved performance only marginally beyond the H1 + H2 model (AUC, 0.890 to 0.892). Our findings are in line

with previous studies of habitat analysis in glioma [26–27], which supports its value for molecular prediction. The stepwise improvement observed across models suggests that habitat-derived radiomics, VASARI features, and the ITH score provide complementary information for IDH prediction. Notably, this performance was achieved using only conventional MRI sequences, without the need for advanced diffusion techniques, additional scan time, or specialized acquisition protocols.

However, VASARI features are ordinal, reader-dependent descriptors, whereas radiomic features are continuous and far finer grained, so the former carry less information per variable. Moreover, the two feature classes may overlap substantially: enhancement quality, margin definition, and the extent of necrosis may already be encoded, indirectly but quantitatively, in habitat texture. SHAP analysis showed that the H1 + H2 radiomics score contributed substantially more to the comprehensive fusion model than the VASARI score, indicating that most predictive information was already captured by habitat-derived radiomics. This finding suggests that habitat radiomics of the edema region capture most of the IDH-related signal available on conventional MRI. VASARI features nonetheless retain practical value because they are transparent, require no computational infrastructure, and can be recorded prospectively by any radiologist.

From a translational perspective, two features of this study support clinical applicability. The models were built exclusively from sequences that form part of the standard preoperative glioma protocol, and their behavior was made transparent by SHAP analysis rather than being left as a black box. The contrasting feature profiles of the two habitats—CE-T1WI and T2WI features in H1 and recurrent dependence entropy features in H2—provide feature-level evidence that the clustering step isolated genuinely different imaging phenotypes rather than arbitrary partitions of a homogeneous region.

Our study had several limitations. First, its retrospective design entails a risk of selection bias, although baseline characteristics did not differ significantly between the two cohorts. Second, the external validation cohort, although derived from two independent centers and different scanner platforms, was of moderate size; larger prospective multicenter studies with protocol harmonization are needed. Finally, we did not assess 1p/19q codeletion and other molecular markers; incorporating these elements is the logical next step.

Conclusion

In conclusion, habitat analysis of the peritumoral edema region on conventional MRI enabled accurate preoperative prediction of IDH status in adult-type diffuse glioma. A comprehensive model combining both habitats with VASARI features and the ITH score achieved favorable performance and generalized to an independent external cohort, which may aid preoperative assessment of IDH status.

Declarations

Ethics approval and consent to participate

This study was performed in accordance with the ethical standards laid down in the 1964 Declaration of Helsinki and its later amendments. Approval was granted by the Medical Ethics Committee of the First Affiliated Hospital of Xinjiang Medical University (approval number: K202405-48). The study was conducted at both participating centers under this approval. The requirement for written informed consent was waived by the Medical Ethics Committee due to the retrospective design of this study.

Consent for publication

Not applicable. All patient data and images were fully anonymized and contain no identifiable information.

Competing interests

The authors declare that they have no competing interests.

Funding

This study was supported by the Scientific and Technological Innovation Leading Talent Program in Tianshan Talents (Grant number 2023TSYCLJ0027).

Author Contribution

S.J.L. and Y.L.W. conceived and designed the study. S.J.L. developed the methodology and drafted the original manuscript. W.Z. and J.M.J. performed the formal analysis and software implementation. W.Z. and S.Y. contributed to data curation. R.X. carried out the investigation and validation. K.H. contributed resources and visualization, and S.Y. contributed to visualization. Y.L.W. supervised and administered the project and critically revised the manuscript. All authors read and approved the final manuscript.

Acknowledgements

Not applicable.

Availability of data and materials

The datasets generated and/or analyzed during the current study are not publicly available due to privacy restrictions and hospital confidentiality policies but are available from the corresponding author on reasonable request.

References

1. Yan Y, Dai W, Mei Q. Multicentric glioma: an ideal model to reveal the mechanism of glioma. Front Oncol. 2022;12:798018. https://doi.org/10.3389/fonc.2022.798018.
2. Louis DN, Perry A, Wesseling P, Brat DJ, Cree IA, Figarella-Branger D, et al. The 2021 WHO classification of tumors of the central nervous system: a summary. Neuro Oncol. 2021;23(8):1231–51. https://doi.org/10.1093/neuonc/noab106.
3. Napel S, Mu W, Jardim-Perassi BV, Aerts HJWL, Gillies RJ. Quantitative imaging of cancer in the postgenomic era: Radio(geno)mics, deep learning, and habitats. Cancer. 2018;124(24):4633–49. https://doi.org/10.1002/cncr.31630.
4. Taweesomboonyat C, Tunthanathip T, Sae-Heng S, Oearsakul T. Diagnostic yield and complication of frameless stereotactic brain biopsy. J Neurosci Rural Pract. 2019;10(1):78–84. https://doi.org/10.4103/jnrp.jnrp_166_18.
5. Fan D, Jiang T, Ma W, et al. CACA guidelines for holistic integrative management of glioma. Holist Integr Oncol. 2022;1:22. https://doi.org/10.1007/s44178-022-00020-x.
6. Verduin M, Primakov S, Compter I, et al. Prognostic and predictive value of integrated qualitative and quantitative magnetic resonance imaging analysis in glioblastoma. Cancers (Basel). 2021;13(4):722. https://doi.org/10.3390/cancers13040722.
7. Yu K, Hu Y, Wu F, Guo Q, Qian Z, Hu W, et al. Surveying brain tumor heterogeneity by single-cell RNA-sequencing of multi-sector biopsies. Natl Sci Rev. 2020;7(8):1306–18. https://doi.org/10.1093/nsr/nwaa099.
8. Beig N, Bera K, Prasanna P, et al. Radiogenomic-based survival risk stratification of tumor habitat on Gd-T1w MRI is associated with biological processes in glioblastoma. Clin Cancer Res. 2020;26(8):1866–76. https://doi.org/10.1158/1078-0432.CCR-19-2556.
9. Lee DH, Park JE, Kim N, Park SY, Kim YH, Cho YH, et al. Tumor habitat analysis by magnetic resonance imaging distinguishes tumor progression from radiation necrosis in brain metastases after stereotactic radiosurgery. Eur Radiol. 2022;32(1):497–507. https://doi.org/10.1007/s00330-021-08204-1.
10. Kazerouni AS, Hormuth DA, Davis T, et al. Quantifying tumor heterogeneity via MRI habitats to characterize microenvironmental alterations in HER2 + breast cancer. Cancers (Basel). 2022;14(7):1837. https://doi.org/10.3390/cancers14071837.
11. Wang X, Xie Z, Wang X, Song Y, Suo S, Ren Y, et al. Preoperative prediction of IDH genotypes and prognosis in adult-type diffuse gliomas: intratumor heterogeneity habitat analysis using dynamic contrast-enhanced MRI and diffusion-weighted imaging. Cancer Imaging. 2025;25(1):11. https://doi.org/10.1186/s40644-025-00829-5.
12. Hagiwara A, Tatekawa H, Yao J, Raymond C, Everson R, Patel K, et al. Visualization of tumor heterogeneity and prediction of isocitrate dehydrogenase mutation status for human gliomas using multiparametric physiologic and metabolic MRI. Sci Rep. 2022;12(1):1078. https://doi.org/10.1038/s41598-022-05077-2.

13. Park JE, Kim HS, Kim N, Park SY, Kim YH, Cho YH, et al. Spatiotemporal heterogeneity in multiparametric physiologic MRI is associated with patient outcomes in IDH-wildtype glioblastoma. Clin Cancer Res. 2021;27(1):237–45. https://doi.org/10.1158/1078-0432.CCR-20-2156.
14. Han S, Liu Y, Cai SJ, Qian M, Ding J, Larion M, et al. IDH mutation in glioma: molecular mechanisms and potential therapeutic targets. Br J Cancer. 2020;122(11):1580–9. https://doi.org/10.1038/s41416-020-0814-x.
15. Zhou Y, Hong T, Qi H, Zhao J, Wu Z, Du J, et al. CT-derived topological intratumoral heterogeneity predicts major pathological response to neoadjuvant immunochemotherapy in resectable non-small-cell lung cancer: a two-center study. Front Immunol. 2026;17:1898208. https://doi.org/10.3389/fimmu.2026.1898208.
16. Luks TL, Villanueva-Meyer JE, Weyer-Jamora C, Gehring K, Jakary A, Hervey-Jumper S, et al. T2 FLAIR hyperintensity volume is associated with cognitive function and quality of life in clinically stable patients with lower grade gliomas. Front Neurol. 2021;12:769345. https://doi.org/10.3389/fneur.2021.769345.
17. Duffau H. White matter tracts and diffuse lower-grade gliomas: the pivotal role of myelin plasticity in the tumor pathogenesis, infiltration patterns, functional consequences and therapeutic management. Front Oncol. 2022;12:855587. https://doi.org/10.3389/fonc.2022.855587.
18. Qiu J, Zhu M, Chen CY, Luo Y, Wen J. Diffusion heterogeneity and vascular perfusion in tumor and peritumoral areas for prediction of overall survival in patients with high-grade glioma. Magn Reson Imaging. 2023;104:23–8. https://doi.org/10.1016/j.mri.2023.09.004.
19. Aoki T, Ohno M, Horiguchi G, Yanagisawa S, Kawauchi D, et al. Prediction of overall survival in glioblastoma using early postoperative reduction in FLAIR lesion volume after gross total resection. Cancers (Basel). 2026;18(10):1585. https://doi.org/10.3390/cancers18101585.
20. Sun C, Fan L, Wang W, Wang W, Liu L, Duan W, et al. Radiomics and qualitative features from multiparametric MRI predict molecular subtypes in patients with lower-grade glioma. Front Oncol. 2021;11:756828. https://doi.org/10.3389/fonc.2021.756828.
21. Ramadas M, Jacob N, Ameratunga M, et al. Unlocking therapeutic synergy: IDH inhibitors and immunotherapy combination in preclinical and clinical IDH mutant glioma models - a systematic review. J Clin Neurosci. 2025;136:111281. https://doi.org/10.1016/j.jocn.2025.111281.
22. Macarulla T, Tabatabai G, Stacchiotti S, et al. Isocitrate dehydrogenase mutations as potential tumour agnostic targets. EJC Suppl. 2026;17:1–10. https://doi.org/10.1016/j.ejcsup.2025.12.002.
23. Xie Y, Li S, Shen N, Gan T, Zhang S, Liu WV, et al. Assessment of isocitrate dehydrogenase 1 genotype and cell proliferation in gliomas using multiple diffusion magnetic resonance imaging. Front Neurosci. 2021;15:783361. https://doi.org/10.3389/fnins.2021.783361.
24. Yamamoto S, Okita Y, Arita H, Sanada T, Sakai M, Arisawa A, et al. Qualitative MR features to identify non-enhancing tumors within glioblastoma's T2-FLAIR hyperintense lesions. J Neurooncol. 2023;165(2):251–9. https://doi.org/10.1007/s11060-023-04454-9.

25. Ohmura K, Tomita H, Hara A. Peritumoral edema in gliomas: a review of mechanisms and management. Biomedicines. 2023;11(10):2731. https://doi.org/10.3390/biomedicines11102731.
26. Zheng WY, Yang RH, Wan ZF, Li H, Ma C, Ouyang QH, et al. MRI-based habitat radiomics for preoperatively predicting IDH status in gliomas. Neurosurg Focus. 2025;59(2):E4. https://doi.org/10.3171/2025.5.FOCUS25135.
27. Liu Y, Wang P, Wang S, Zhang H, Song Y, Yan X, et al. Heterogeneity matching and IDH prediction in adult-type diffuse gliomas: a DKI-based habitat analysis. Front Oncol. 2023;13:1202170. https://doi.org/10.3389/fonc.2023.1202170.

Figures

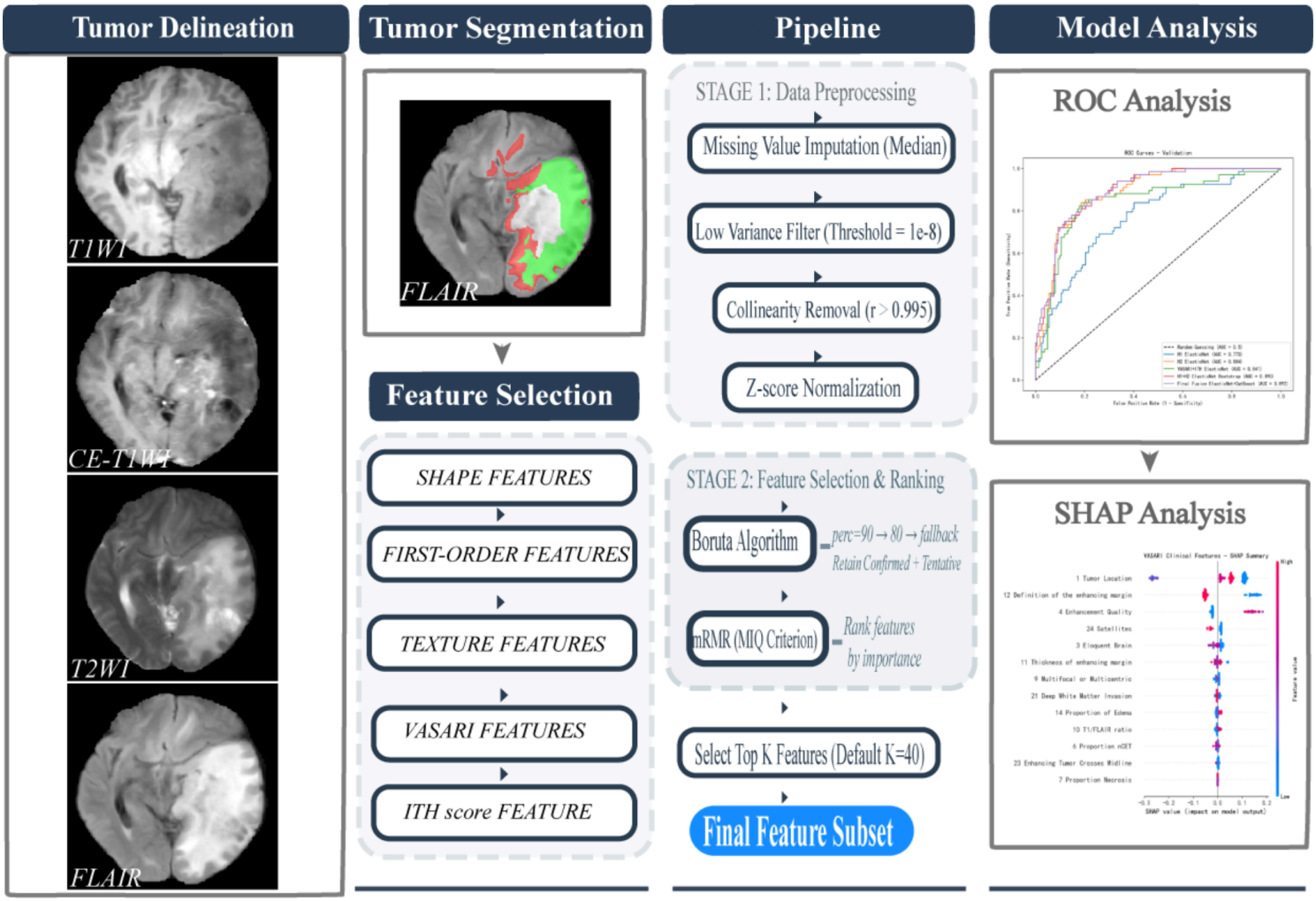

Figure 1

Study workflow. After patient enrollment, conventional MRI underwent preprocessing and segmentation of the peritumoral edema region. *K*-means clustering partitioned the edema region into two habitats (H1 and H2), from which habitat-based radiomic features were extracted. These features were integrated with VASARI features and the intratumoral heterogeneity (ITH) score to develop five machine-learning

models, followed by validation and SHAP-based interpretability analysis. MRI magnetic resonance imaging, VASARI Visually Accessible Rembrandt Images, ITH intratumoral heterogeneity, SHAP Shapley additive explanations

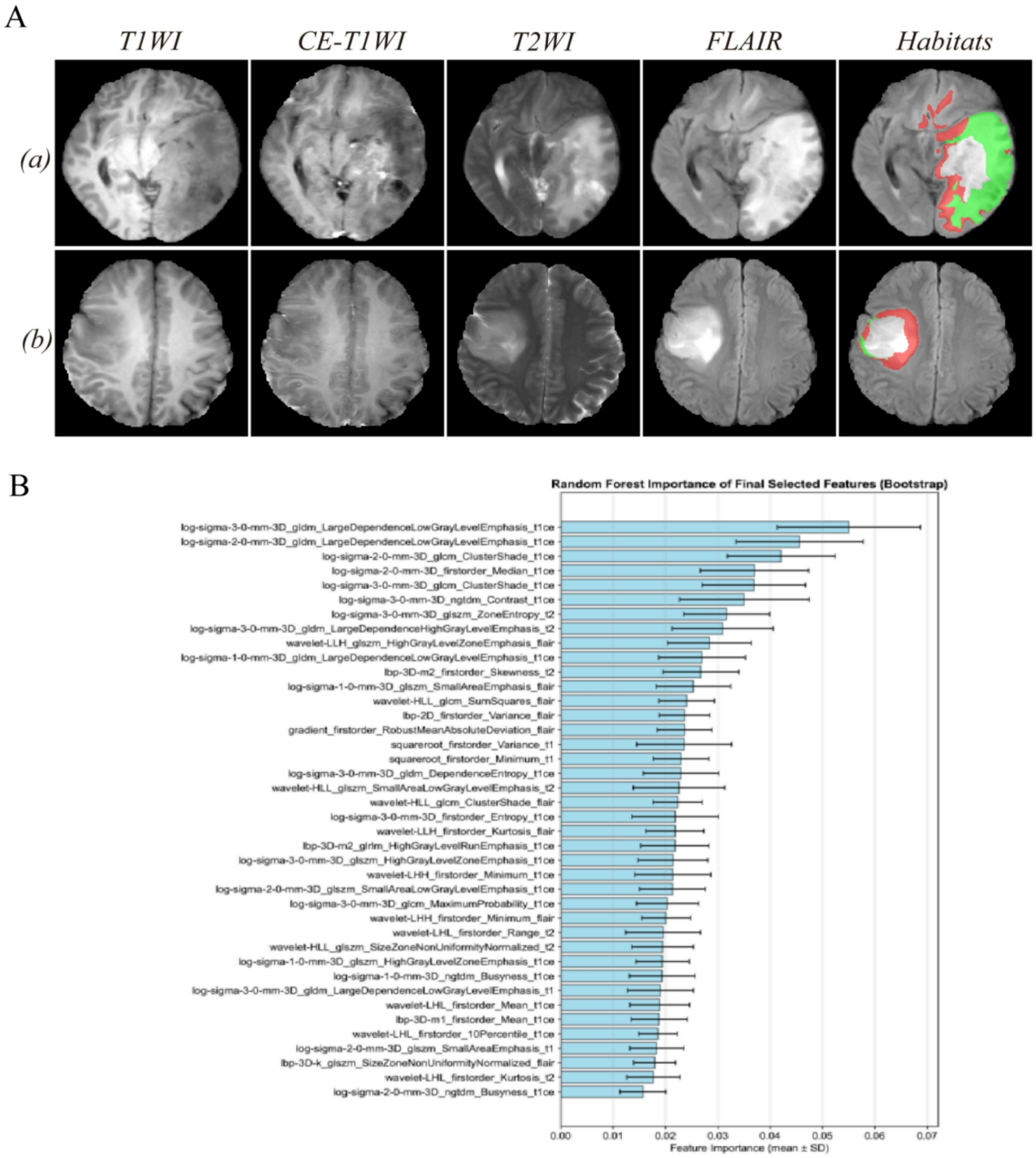

Figure 2

Habitat analysis and feature selection. **A** Representative habitat maps of the peritumoral edema region, with red indicating habitat H1 and green indicating habitat H2. **B**The 40 retained radiomic features, ranked by random forest importance

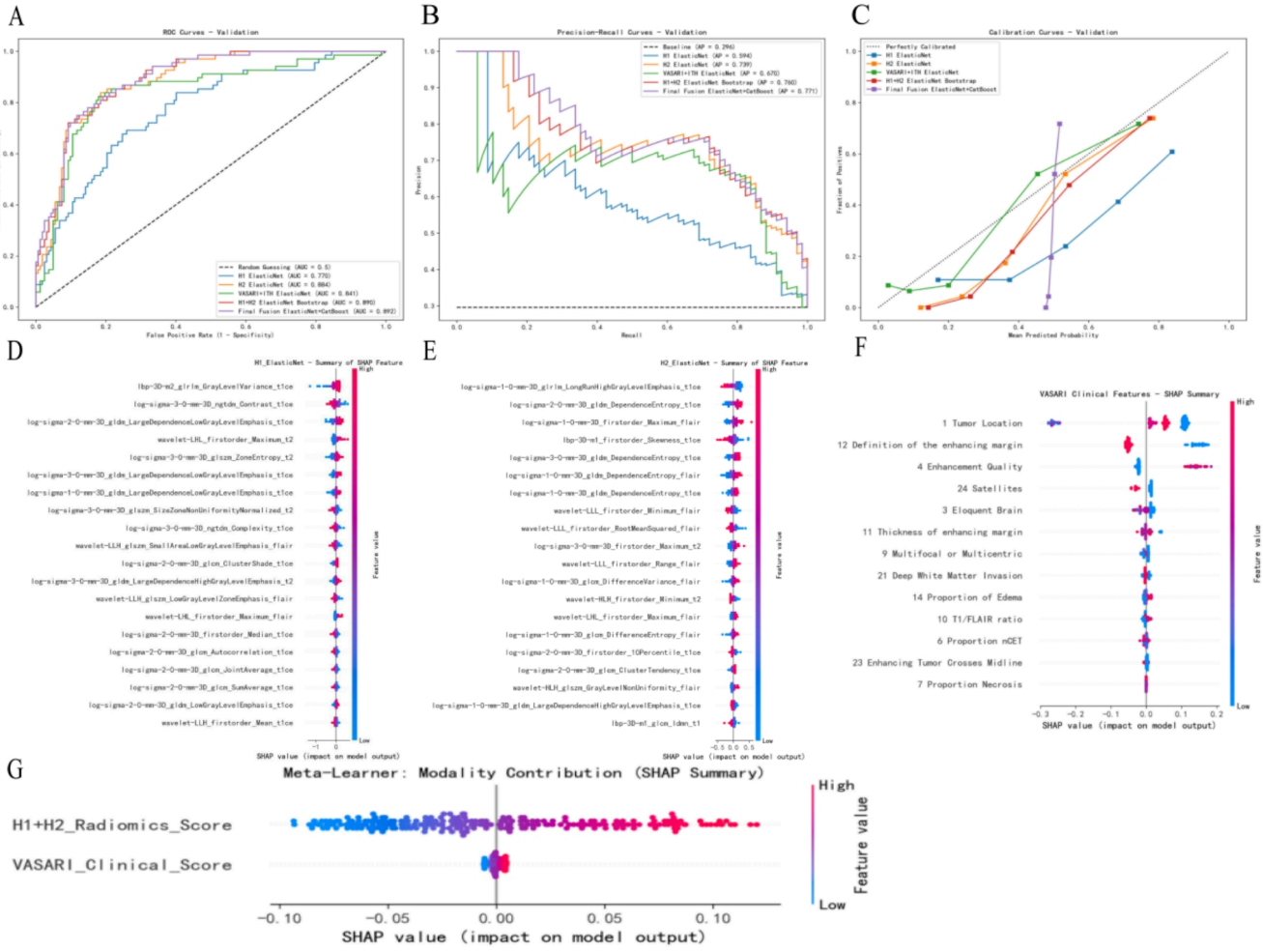

Figure 3

Model performance and interpretability. **A** Receiver operating characteristic curves, **B** precision-recall curves, and **C** calibration curves of the five models in the validation set. SHAP summary plots for **D**the H1 habitat model, **E** the H2 habitat model, **F** the VASARI + ITH model, and **G** the comprehensive fusion model, showing the relative contributions of the H1 + H2 radiomics score and the VASARI score